

Article

Demand-Based Control Design for Efficient Heat Pump Operation of Electric Vehicles

Dominik Dvorak * , Daniele Basciotti and Imre Gellai

Center for Low-Emission Transport—Electric Drive Technologies, AIT Austrian Institute of Technology GmbH, 1210 Vienna, Austria; daniele.basciotti@ait.ac.at (D.B.); imre.gellai@ait.ac.at (I.G.)

* Correspondence: dominik.dvorak@ait.ac.at

Received: 13 August 2020; Accepted: 14 October 2020; Published: 19 October 2020



Abstract: Thermal management systems of passenger vehicles are fundamental to provide adequate cabin thermal comfort. However, for battery electric vehicles they can use a significant amount of battery energy and thus reduce the real driving range. Indeed, when heating or cooling the vehicle cabin the thermal management system can consume up to 84% of the battery capacity. This study proposes a model-based approach to design an energy-efficient control strategy for heating electric vehicles, considering the entire climate control system at different ambient conditions. Specifically, the study aims at reducing the energy demand of the compressor and water pumps when operating in heat pump mode. At this scope, the climate control system of the reference vehicle is modelled and validated, enabling a system efficiency analysis in different operating points. Based on the system performance assessment, the optimized operating strategy for the compressor and the water pumps is elaborated and the results show that the demand-based control achieves up to 34% energy reduction when compared to the standard control.

Keywords: modelling and simulation; heat pump; demand-based control; operating strategy; efficiency

1. Introduction

1.1. Background and Problem

In recent years, electric mobility is becoming more popular and this is underlined by the fact that all big companies in the automotive industry have electric vehicles in their portfolio [1]. However, one big challenge of battery electric vehicles (BEVs) is represented by the driving range limitation due to the battery capacity constraints [2,3]. During the past years there have been many scientific studies and publications dealing with driving range anxiety [4,5], trying to overcome these limitations.

1.2. Previous Research in the Field

Thermal management is essential for ensuring adequate thermal comfort in passenger vehicles. Shete and Farrington et al. (respectively, in [6,7]) studied the negative impact of the air conditioning systems for internal combustion engine (ICE) vehicles on fuel consumption and CO₂ emissions. One major disadvantage related to the climate control system, also called heating, ventilation, and air conditioning (HVAC) system later in the paper, of BEVs compared to conventional ICE vehicles is the unavailability of waste heat from the engine for heating purposes. Instead, BEVs must drain the energy from the battery for heating, thus impacting negatively the vehicle range [8]. Indeed, the importance of thermal management optimization is highlighted by the fact that heating in cold winter conditions or cooling in hot summer conditions can increase the energy consumption from the HVAC system up to 84%, resulting in a significant reduction of the maximum driving range of the vehicle up to

60% [9]. Additionally, high cycling rates of the battery lead to faster degradation and in turn to higher maintenance costs for the owners [10–16].

The challenge of reducing energy demand for the climate control system is approached by designing and testing new systems and components [17–27] by means of prototyping and real-life tests, which are time consuming and resources demanding at the same time.

Zhang et al. [17] designed and investigated the performance of an EV heat pump system. Rabl et al. [18] compared a heat pump system with an electric air heater system for an EV. Ozbek et al. [19] introduced an efficient water-to-water heat pump system, which can utilize waste heat from the powertrain cooling circuit for cabin heating. Lajunen [20] in his study achieved a decrease up to 4% for the vehicle energy consumption by combining a heat pump system and waste-heat recovery from the powertrain components. Weustenfeld et al. [21] proposed and validated on a simulation base a secondary loop heating and cooling system to simplify the vehicle front end and at the same time to efficiently cool down and heat up the passenger cabin. In their paper, Osborne et al. [22] provided an overview about currently existing thermal management strategies and their impacts. Suh et al. [23] designed a heat pump system with waste-heat recovery for a bus, with required cooling and heating capacities of 28 kW and 26 kW, respectively. Leighton [24] suggested combining the cooling circuit for the battery with the water cycle for the cabin heating. With his HVAC system he achieved a range increase of 9%. In their contribution, Kitanoski and Hofer [25] developed an optimization methodology for exemplarily optimizing the fan speed and pump speed of a single cooling loop at the same time, however without considering the entire HVAC system. Fischer et al. [26] compared for a fuel-cell vehicle their heat pump system to an HVAC system using electrical heater. De Nunzio et al. [27] followed a holistic approach, however evaluating their heat pump system only for an ambient temperature of $-10\text{ }^{\circ}\text{C}$. Moreover, Hosoz and Direk [28] investigated the impact of reducing the air-inlet temperature on the performance of a heat pump system, considering solely the refrigerant cycle in their optimizations.

Alternatively, at the scope of increasing the efficiency and/or reducing the loads of climate control, several studies tried to optimize the systems on a simulation based from the control strategy perspective [29–31]. Al Faruque and Vatanparvar [29] illustrated in their study how automotive climate controls work and the benefits gained by system modelling and estimation for different conditions in terms of battery lifetime and driving range. Hendricks [30] developed the SINDA/FLUINT analysis software, which captures all the relevant physics of transient climate control system performance and integrates a simplified cabin thermal model demonstrating the powerfulness of the model-based system design optimization. Moreover, Lee et al. [31] in their study demonstrated the high potential of energy savings and COP improvements by implementing a saturation cycle concept (four-stage cycle with two-phase refrigerant injection) which could improve the system efficiency by 23.9% and reduce the power consumption by 19.3%.

However, in the above-mentioned studies either simplifications for the HVAC system modelling were made, the investigations were limited to the refrigerant-cycle optimization or the systems were only investigated at one single ambient temperature.

1.3. Current Study Novelties and Focus

This paper follows a model-based approach to optimize the operating strategy of the compressor and the water pumps of a heat pump system for EVs. The improvements are achieved by a demand-based design of the control strategy where the components are optimally operated in part load conditions.

The abovementioned studies from Kitanoski and Hofer [25], De Nunzio et al. [27], and Hosoz and Direk [28] deal with similar topics like this study. However, this study differs from the existing studies in two key aspects. On the one hand, the paper investigates the optimal demand-based control of compressor and water pumps for various operating points, deriving the optimal strategy at different ambient conditions. On the other hand, the optimal operating points are analyzed using the developed simulation models which include not only the refrigerant cycle but also the entire HVAC system

components. The optimal strategy is obtained considering the performance of the entire system by varying the target air outlet temperature of the HVAC system and the pump speeds.

To validate the proposed approach, the study compares in terms of energy consumption the standard control strategy scenario with three incremental improvement scenarios based on three control mechanisms and quantifies the energy-saving potential at different ambient conditions.

2. Methodology

The optimal demand-based control has been developed and tested in a virtual environment based on a parametric variation. Indeed, compared to the real-life testing the model-based approach reduces the development time for optimizing the controls of the proposed components.

The system model used for the optimization process includes the HVAC model, the 1D thermal cabin model, and the control system as shown in Figure 1. The details of the sub-models are given in Sections 2.1 and 2.2. The models are implemented in Dymola/Modelica using models from the Modelica Standard Library [32] and from the TIL Suite [33]. The parameters for each of the sub-models are derived either from the available measurement data (see Section 2.3) or from technical datasheets. The model validation results are provided in Section 3.1.

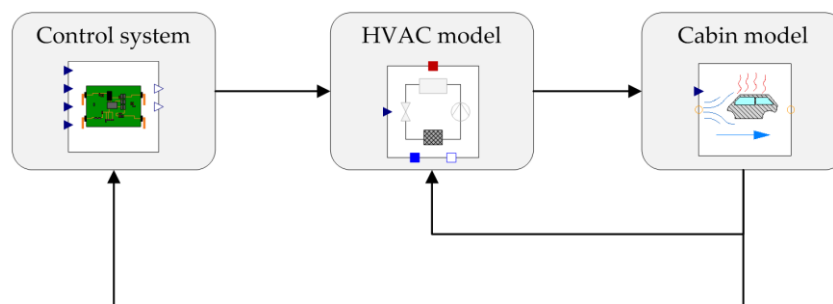


Figure 1. Schematic overview of system model.

In this work, four different scenarios for heat pump operation are analyzed under relevant ambient conditions:

- Reference scenario (**Control Base**),
- 1st improvement step: load controlled-compressor scenario with demand-dependent air-outlet-temperature setpoint of the HVAC system (**Control Step 1**),
- 2nd improvement step: load controlled-water-pumps scenario with demand-dependent speed of the water pumps (**Control Step 2**),
- 3rd improvement step: combination of steps 1 and 2 (**Control Step 3**).

The proposed methodology, represented in Figure 2, develops an enhanced and efficient operating strategy for the compressor and the two water pumps in a virtual environment. Thereby, it offers a reduced development time when compared to real-life testing and it proposes how to determine the optimum load setpoints of the proposed components.

The methodology includes the following steps:

1. System identification and modelling in an iterative process: models and measured data from the real-world system have been used for the parametrization;
2. HVAC-compressor and water-pumps controller analysis and synthesis: identification of the dynamic characteristics of the system model and definition of an appropriate controller;
3. Ambient temperature variation: simulation allows the investigation under various conditions to find the optimal setpoints;
4. Determination and extrapolation of the demand-based optimal operating points of the HVAC compressor and the water pumps at various boundary conditions;

5. Deployment and validation of the developed component control strategy by quantifying the improvement potentials of the measures.

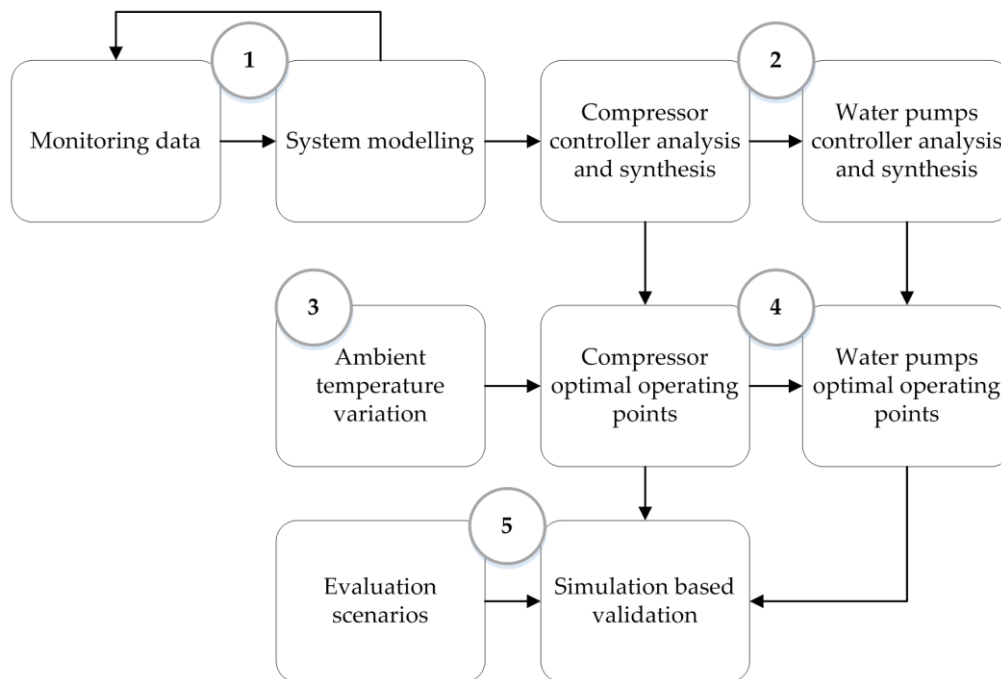


Figure 2. Schematic overview of the methodology.

To find the optimal setpoints at different ambient conditions, a parameter variation is performed. An overview of the boundaries is given in Table 1. Although the climate control system is capable of operating in both heating and cooling mode, the study focuses on heat pump mode, and the assessment is performed at an ambient temperature of $-10\text{ }^{\circ}\text{C}$ to $10\text{ }^{\circ}\text{C}$ in steps of $5\text{ }^{\circ}\text{C}$ with the condenser temperature setpoint varied continuously between $22\text{ }^{\circ}\text{C}$ and $70\text{ }^{\circ}\text{C}$ and the speed of both water pumps varied continuously between 5 Hz and 100 Hz .

Table 1. Parameter variation table.

	Heat Pump Mode
Cabin air inlet temperature [$^{\circ}\text{C}$]	[22–70]
Speed of water pump on condenser side [Hz]	[5–100]
Speed of water pump on evaporator side [Hz]	[5–100]
Ambient temperature [$^{\circ}\text{C}$]	[−10, −5, 0, 5, 10]

2.1. 1D Thermal Cabin Model

A schematic overview of the cabin model is provided in Figure 3. The 1D thermal cabin model uses an object-oriented approach and includes heat exchange mechanism of conduction and convection to the ambient. Under steady state conditions, the energy equations for car cabin thermal equilibrium can be written as:

$$Q_{\text{losses}} = Q_{\text{heat}} = Q_{\text{trans}} + Q_{\text{ven}} + Q_{\text{rad}} + Q_{\text{met}} \quad (1)$$

where Q_{losses} are the overall heat losses between the cabin and ambient and are balanced with the energy provided by the climate control system (Q_{heat}). The overall heat losses of the cabin can be divided into:

- Q_{trans} [W], transmission losses through the body of the cabin;

- Q_{vent} [W], ventilation losses through the air leakage of the cabin (depending strongly on the operation mode: fresh air or recirculated air);
- Q_{rad} [W], solar radiation load gain (excluded from the study to reduce the complexity otherwise introduced by a large number of combinations between ambient temperature and solar radiation conditions);
- Q_{met} [W], metabolic load from the passengers (excluded from the study for the same reason of the solar radiation).

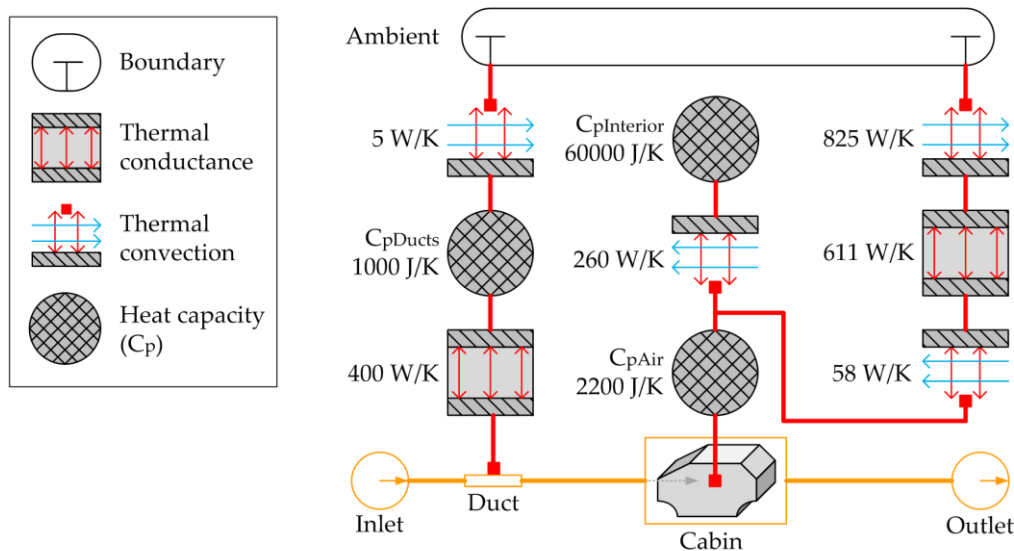


Figure 3. Cabin model schematic overview.

The components of the energy equations (1) can be written as:

$$Q_{\text{trans}} = k_{\text{cab}} A_{\text{cab}} (T_{\text{cab}} - T_{\text{amb}}) \quad (2)$$

$$Q_{\text{ven}} = m_{\text{in}} c_{p\text{Air}} (T_{\text{vent}} - T_{\text{amb}}) \quad (3)$$

where:

- k_{cab} [W/K.m²], overall heat-loss coefficient of the cabin;
- A_{cab} [m²], overall external area of the cabin;
- T_{cab} [K], average cabin temperature;
- T_{amb} [K], ambient temperature;
- m_{in} [kg/s], volume flow of the fresh air into the cabin;
- $c_{p\text{Air}}$ [J/kg.K], thermal capacity of the air;
- T_{vent} [K], exhaust air temperature through the air leakages of the cabin.

The temperature of the cabin, calculated in the heat capacity of the cabin air ($c_{p\text{Air}}$), is therefore the result of the energy flow between indoor and ambient air through conduction and convection phenomena as reported graphically in Figure 3. The presented parameters have been estimated from measurement- and material data. Conduction, convection, and heat capacity models are taken from the Modelica Standard Library. Additionally, for the realistic behavior of the system, the ventilation ducts have been considered and modelled including heat losses through conduction and convection and heat capacity of the duct itself.

Specifically, the air path (orange) starts at the inlet and leads through the ducts to the cabin-air volume and finally to the outlet. The thermal connections of the model are represented by the red lines. From the inside wall surfaces of the ducts, thermal energy is conducted through the wall to a heat

capacity (thermal point mass). From there, the thermal energy is also dissipated to the ambient via convective heat transfer. The air within the cabin is convectively transferred to the heat capacity of the interior parts, such as the seats or the dashboard. In addition, thermal energy is transferred through the chassis to the ambient. Thereby, the heat flow is determined by convective heat transfer between the cabin inside air and the chassis, thermal conduction through the chassis and finally convective heat transfer between the outside of the chassis and the ambient.

2.2. HVAC System and Control System

A schematic overview for the implemented propane-based (R290) HVAC system model is depicted for both cooling mode and heat pump mode in Figure 4. The models are implemented in Dymola/Modelica using models from the TIL Suite. Details of the mathematical models of the single components are reported in [33].

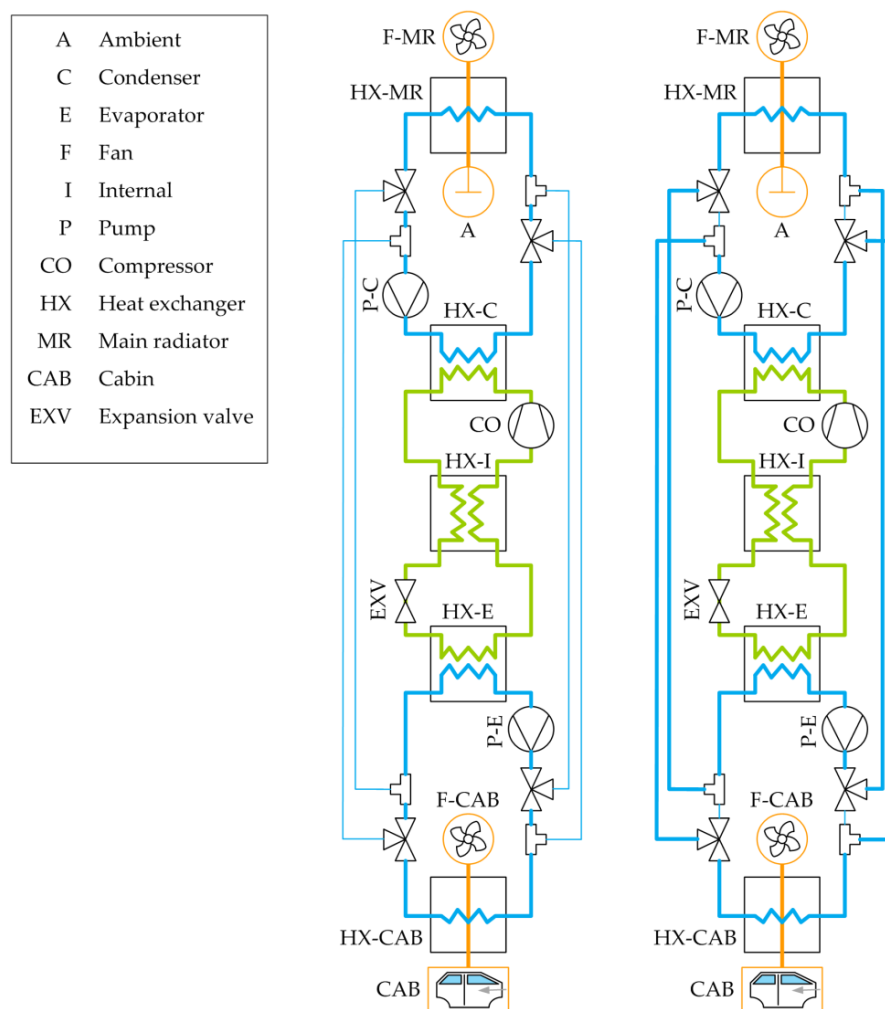


Figure 4. Heating, ventilation, and air conditioning (HVAC) system model schematic overview: cooling mode (left) and heat pump mode (right).

The model is divided into three parts: refrigerant (in green), coolant (in blue), and air cycles (in orange). The refrigerant cycle is based on R290 and considers the compressor, condenser, internal heat exchanger, expansion valve, and evaporator. The coolant cycle is based on water-glycol at a mass-fraction of 50% each and consists of the water side of the condenser, evaporator and front heat exchanger (main radiator), pumps and valves. By switching the coolant cycle valves, the refrigerant cycle can be either used in cooling or in heat pump mode, cp. Figure 4 left and right, respectively. The

air cycle considers the front heat exchanger, the cabin heat exchanger, the main radiator fan, and cabin fan and a cabin model.

For the evaluation of the performance of the system the following key performance indicators (KPIs) have been considered when comparing the scenarios:

- Electrical power consumption $P_{\text{electricalSys}}$ [W], as the electrical energy demand of the entire HVAC system (consisting of compressor, water pumps and cabin fan);
- Average cabin temperature;
- Coefficient of performance (COP and COP_{sys}), related to the heating mode and determined as:

$$\text{COP} = Q_{\text{condenser}}/P_{\text{electrical}} \quad (4)$$

$$\text{COP}_{\text{sys}} = Q_{\text{condenser}}/P_{\text{electricalSys}} \quad (5)$$

with:

- $Q_{\text{condenser}}$ [W], thermal energy output of the condenser on the refrigerant side;
- $P_{\text{electrical}}$ [W], the electrical energy of the compressor.

The base control algorithms (**Control Base**) for the five main components are described in the following section and depicted in Figure 5.

- **Compressor:** a PI (proportional-integral) controller controls the compressor speed to keep the target air temperature to be supplied by the HVAC system (T_{inTarget}) at a constant value of 70 °C;
- **Expansion valve (EXV):** a PI controller ensures that no liquid refrigerant is sucked into the compressor by keeping the superheat temperature (T_{sh}) of the refrigerant after the evaporator at 5 K;
- **Cabin fan:** a PI controller regulates the air mass flow of the cabin fan via the fan voltage to keep the cabin temperature (T_{cab}) at a specific target value, which was considered 22 °C in the study;
- **Water pumps (condenser and evaporator):** constant pump speed on the condenser and evaporator side were set corresponding to the design point at −10 °C.

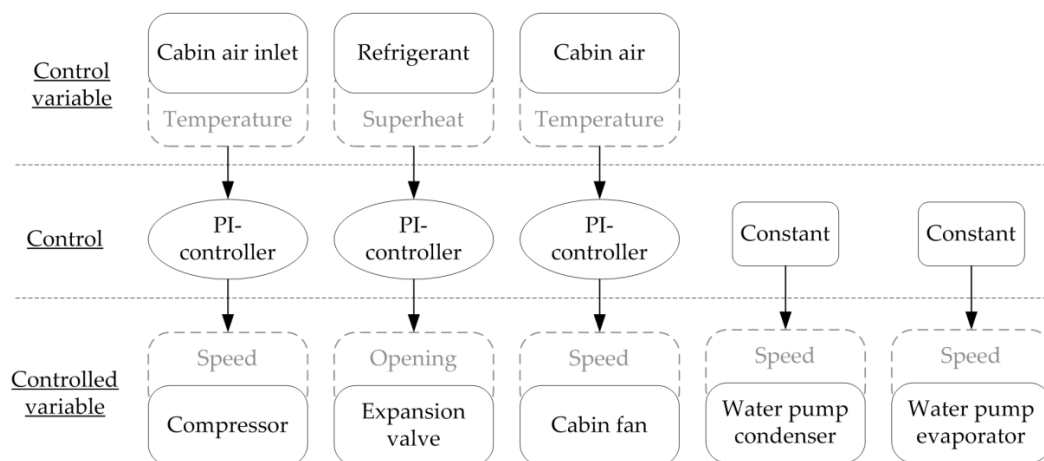


Figure 5. Schematic overview of the base control dependencies of the main HVAC components.

2.3. Models Parametrization

In the first step, each single component of the HVAC system, for which measurement data were available, has been parameterized separately. Figure 6 shows the workflow from the monitoring data up to the system model. First, monitoring data were used to analyze the components and to choose the appropriate ones from the available libraries. Second, a comparison between results and monitoring

data was used to extract component parameters, with the target of reducing simulation model errors. The parameters for sub-models, for which measurement data were not available, were taken from technical datasheets.

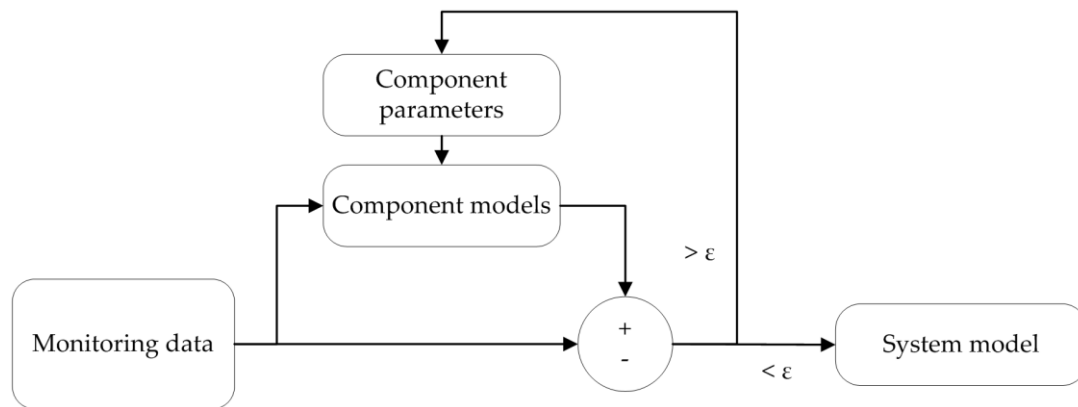


Figure 6. Model parametrization schematic overview.

2.4. Demand-Based Control Design

Although the implemented HVAC system model is capable of simulating both cooling and heat pump mode, this study focuses only on heat pump mode. At lower ambient temperatures, the HVAC system must provide higher heating power to compensate the difference between ambient temperature and target cabin air temperature. Therefore, the heating demand of the heat pump system increases with a decrease in ambient temperature. This, in turn, means that the design of the demand-based control for the HVAC system needs to consider the dependency of the ambient temperature on the heating demand.

The developed system model has been used to investigate the behavior of the HVAC system in further operating points which have not been measured. The main advantages of the proposed model-based approach are therefore related to the development-time efficiency (simulations are largely faster than measurements) and the safety aspects (hardware and software modifications are applied to models which, when working outside their operating range, cannot get damaged). The analysis for the demand-based control design has been performed for three different components (see Figure 4) in three consecutive steps:

- **Control Step 1:** compressor,
- **Control Step 2:** water pump on condenser side, water pump on evaporator side,
- **Control Step 3:** combination of all measures.

The base control strategy of the main components of the HVAC system, which has been described in chapter 2.2, serves as the reference scenario and is summarized in Table 2. Thereby, “PI” means that the quantity is controlled by a PI controller and “ $f(x)$ ” expresses a dependency upon the variable “ x ”. As before the optimization the system performance is not known entirely, $T_{inTarget}$ was chosen high enough to guarantee appropriate heat-up and the pumps run at higher speeds than necessary, to be on the safe side. In order to determine the demand-dependent optimum control of the components, $T_{inTarget}$ and the speed of the pump on the condenser side ($n_{pumpCond}$) and on the evaporator side ($n_{pumpEvap}$) have been varied using ramp profiles at different ambient temperatures. The simulation is terminated either after the ramps have reached their final values at 10000 s or when the target cabin temperature of 22 °C can no longer be assured (i.e. when T_{cab} falls below 22 °C in steady state). The simulations have been repeated for different ambient temperatures, ranging from −10 °C to 10 °C.

Table 2. Component control for demand-based system analysis.

Component	Quantity	Control Base	Control Step 1	Control Step 2	
Target air supply	Temperature	Constant	Ramp	$f(T_{amb})$	$f(T_{amb})$
Compressor	Speed	$PI = f(T_{in})$	$PI = f(T_{in})$	$PI = f(T_{in})$	$PI = f(T_{in})$
Expansion valve	Opening	$PI = f(T_{sh})$	$PI = f(T_{sh})$	$PI = f(T_{sh})$	$PI = f(T_{sh})$
Water pump condenser	Speed	Constant	Constant	Ramp	Constant
Water pump evaporator	Speed	Constant	Constant	Constant	Ramp
Cabin fan	Speed	$PI = f(T_{cab})$	$PI = f(T_{cab})$	$PI = f(T_{cab})$	$PI = f(T_{cab})$

As the compressor controls $T_{inTarget}$, the operation of the compressor can be optimized by adapting this value. Therefore, in **Control Step 1** of the demand-based control design, a ramp starting from 70 °C and decreasing to 22 °C within 10,000 s has been used to find the optimum value for $T_{inTarget}$ at different ambient temperatures. In **Control Step 2**, $n_{pumpCond}$ and $n_{pumpEvap}$ are varied, respectively, using a ramp profile changing from 100 Hz to 5 Hz within 10,000 s. The optimum $T_{inTarget}$, $n_{pumpCond}$ and $n_{pumpEvap}$ for each of the analyzed ambient temperatures have been stored in a lookup table. **Control Step 3** combines the results of **Control Steps 1** and **2**. Table 3 summarizes the ramp parameters that have been used for parameter variation.

Table 3. Summary of the parameter variation using ramp profiles.

Control Step	Component	Variation Variable	Start Value	End Value	Duration
1	Compressor	$T_{inTarget}$	70 °C	22 °C	10,000 s
2	Pump condenser	$n_{pumpCond}$	100 Hz	5 Hz	10,000 s
	Pump evaporator	$n_{pumpEvap}$	100 Hz	5 Hz	10,000 s

The target of the variation study is to find the operating point for the three components at different T_{amb} where the target cabin temperature of 22 °C can still be kept and where the electrical power consumption of the HVAC system is at a minimum. Table 2 summarizes the component control strategies and dependencies of the main components for the different steps of the demand-based system analysis. The results and analysis of the variation simulation is reported in chapter 3.2.

3. Results

This section describes the results of the study and consists of three parts. First, the validation of the developed simulation models is reported. Second, the results for the demand-based control strategy, which has been elaborated using the above-mentioned methodology, is described. Finally, the performance of a representative HVAC system using the developed control strategies (**Control Steps 1, 2 and 3**) is analyzed and compared to the reference case using a non-optimized control strategy (**Control Base**).

3.1. Models Validation

The 1D thermal cabin model, developed within the framework of the QUIET project [34], has been validated against measurement data in heating mode operation. The available measurement dataset corresponds to the heat-up phase with the maximum power at an ambient temperature of 20 °C. The cabin fan was at maximum level and the provided air temperature at the cabin heat exchanger was 55 °C. Figure 7 shows the comparison of the measurements (dashed) and the simulation (solid). The results illustrate that the 1D thermal cabin model can accurately reproduce the air temperature within the cabin. Indeed, the cabin temperature prediction at steady state conditions (after 4000 s) has an error of 0.44 °C or 1%. Moreover, the transient behavior of the simulated cabin temperature is predicted well with a standard deviation of 1.55 °C or 5.3%.

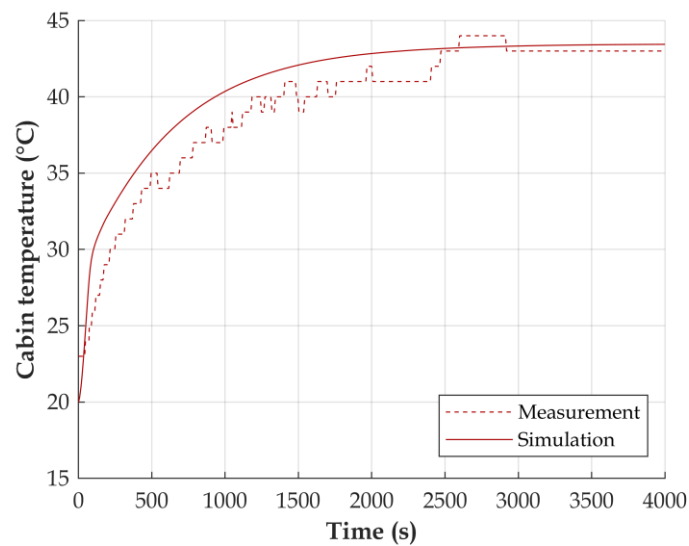


Figure 7. Measured and simulated cabin temperature at maximum heating power.

Subsequently, the total refrigerant cycle has been validated against measurements for one representative operating point, e.g., at an ambient temperature of $-10\text{ }^{\circ}\text{C}$. The validation results of the refrigerant-cycle model on the pressure-enthalpy (p,h) diagram can be seen in Figure 8 where the grey line represents the saturation line of propane, the dashed line the measurements, and the solid line the corresponding simulation results. In the investigated operating point of the validation case, the compressor model has a deviation in the efficiency, resulting in a maximum enthalpy error of about 19 kJ/kg or 2.4% compared to the measurements. However, they represent only minor deviations when considering the complexity of the HVAC system, i.e., the simulation results are in good accordance with the measurements for the operational point under consideration.

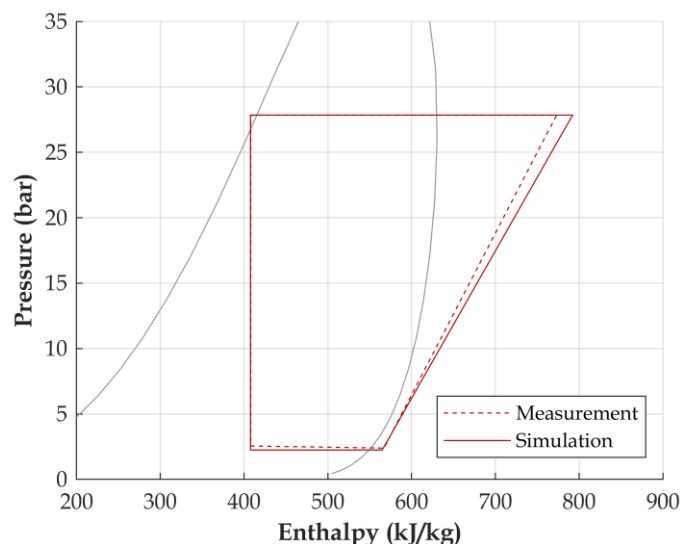


Figure 8. p,h diagram of the measured and simulated total HVAC system in heat pump mode.

3.2. Demand-Based Control Strategy

The power consumption of the HVAC system at different ambient temperatures and T_{in} is represented in Figure 9. The crosses mark the operating points with the lowest energy consumption in each scenario. At high cabin inlet temperatures, the compressor needs to provide high heating power. Starting from the highest temperature (70 °C), the trends of the lines show that the power consumption first decreases with reduced cabin inlet temperature because the compressor needs to provide high heating capacity. When T_{in} is further decreased, at a specific point the power consumption starts to rise again. This can be explained by the fact that the controller of the cabin fan tries to keep the cabin temperature at the setpoint, which is 22 °C. When T_{in} decreases, the fan must provide a higher air mass flow, in order to compensate the lower air temperature and therefore the power consumption starts to increase. Additionally, as the system operates in fresh-air mode, the amount of air that is blown out of the vehicle is increased with higher fan levels, which in turn leads to higher ventilation losses and therefore power consumption.

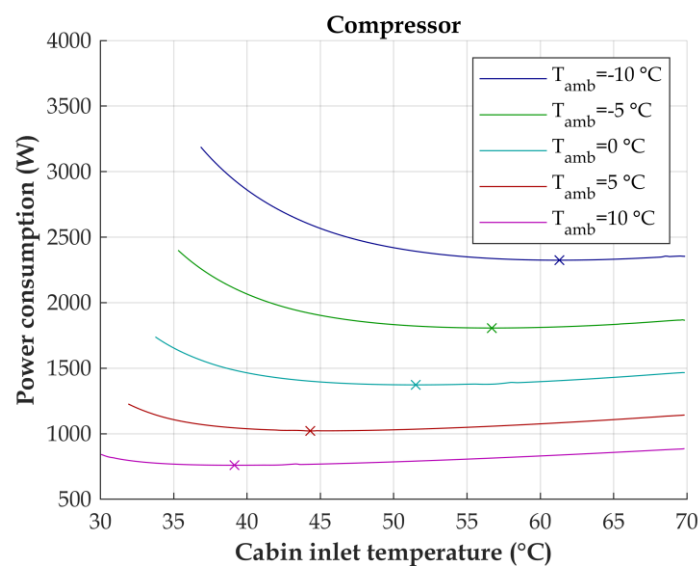


Figure 9. Optimum cabin inlet temperature at different ambient temperatures.

Figure 10 shows the condenser water pump speed optimization with a similar trend comparable to the compressor. For high pump speeds, the power consumption of the entire HVAC system is high. Toward lower pump speeds the power consumption decreases until it reaches an optimum operating point. Then, when further decreasing the pump speed, the overall power consumption rises again. At very low pump speeds, the slope of the power consumption significantly increases. This can be explained by the fact that the mass flow in the water cycle gets too low to transmit the thermal energy from the refrigerant cycle to the cabin heat exchanger and thus the target inlet air temperature cannot be reached. Consequently, the PI controller of the compressor increases the compressor speed. At the same time, the PI controller of the cabin fan increases the fan speed to compensate the reduced temperature at the air inlet, thus increasing also the ventilation losses.

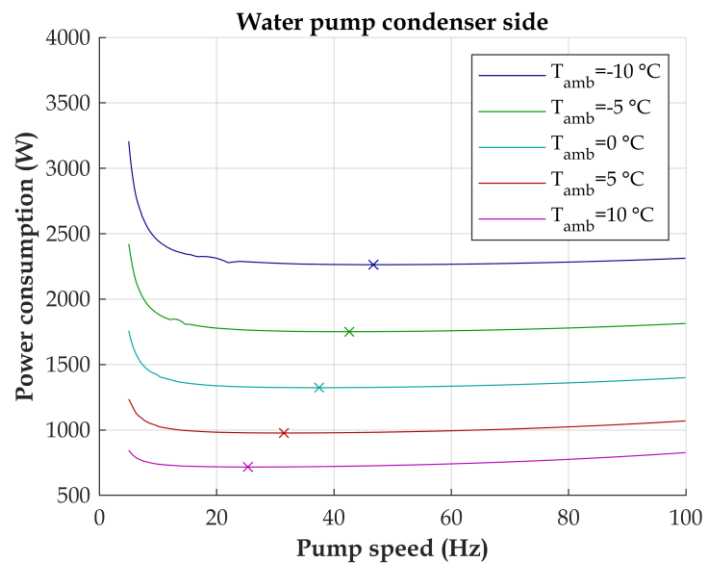


Figure 10. Optimum condenser pump speed at different ambient temperatures.

Figure 11 compares the power consumption of the HVAC system when varying the speed of the water pump on evaporator side at different ambient temperatures. The charts show a similar trend like for the water pump on condenser side but with slightly flatter slope, especially at lower pump speeds.

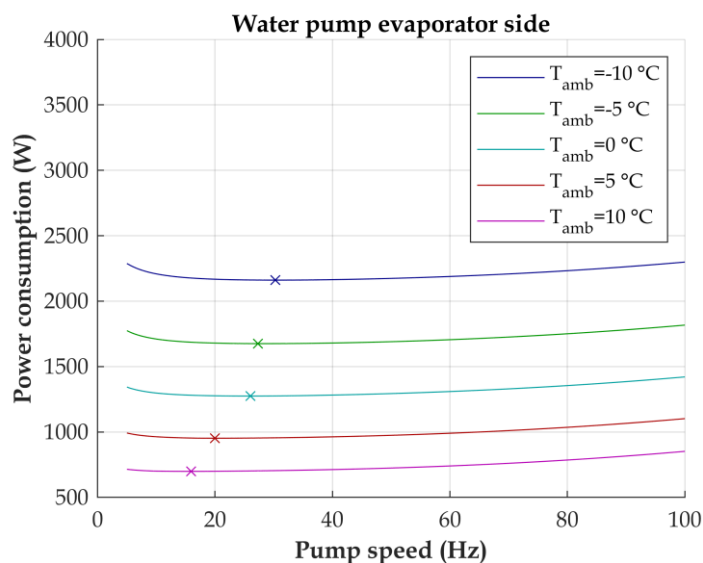


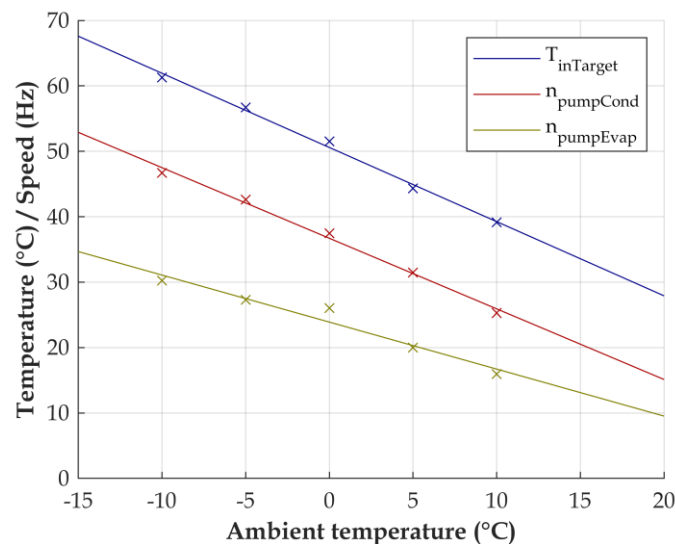
Figure 11. Optimum evaporator pump speed at different ambient temperatures.

Table 4 summarizes the results of the study. As the study showed, the heating demand of the HVAC system depends strongly on the ambient temperature. Therefore, the demand-based control (**Control Step 3**) replaces the constant control values from the base control (**Control Base**) with values, which depend on T_{amb} , to achieve better efficiency.

Table 4. Base control compared to demand-based control of the HVAC system.

Component	Controlled Variable	Control Base	Control Step 3
Target air supply	Temperature	Constant	$f(T_{amb})$
Compressor	Speed	$PI = f(T_{in})$	$PI = f(T_{in})$
Expansion valve	Opening	$PI = f(T_{sh})$	$PI = f(T_{sh})$
Water pump condenser	Speed	Constant	$f(T_{amb})$
Water pump evaporator	Speed	Constant	$f(T_{amb})$
Cabin fan	Speed	$PI = f(T_{cab})$	$PI = f(T_{cab})$

Figure 12 presents the proposed control functions for the demand-based control. As already mentioned earlier, the heating demand for the HVAC system strongly depends on the ambient temperature. Therefore, the optimum operating points, which have been found above (see crosses in Figure 12), are correlated with the ambient temperature. A clear linear dependency between all three quantities (T_{in} , $n_{pumpCond}$ and $n_{pumpEvap}$) and T_{amb} can be seen. Therefore, a linear function has been fit through the extracted operating points. The same function has been used to extrapolate the functions also down to $-15\text{ }^{\circ}\text{C}$ and up to $20\text{ }^{\circ}\text{C}$ ambient temperature.

**Figure 12.** Control tables for demand-based control of the compressor and the water pumps.

3.3. Use Case Results

The impact of the demand-based control of the HVAC system has been evaluated at different ambient temperatures. Figure 13 compares the COP of the climate control system for the various scenarios. As described in (4), the COP represents the efficiency with respect to only the compressor power consumption. In this case Figure 13 shows that, as expected, the efficiency increases with increasing ambient temperature, since the temperature lift between the source (evaporator) and the sink (condenser) is reduced. However, for a correct evaluation of the impact of the control strategies it is required to compare them related to the entire HVAC system and not only limiting the evaluation to the refrigerant cycle.

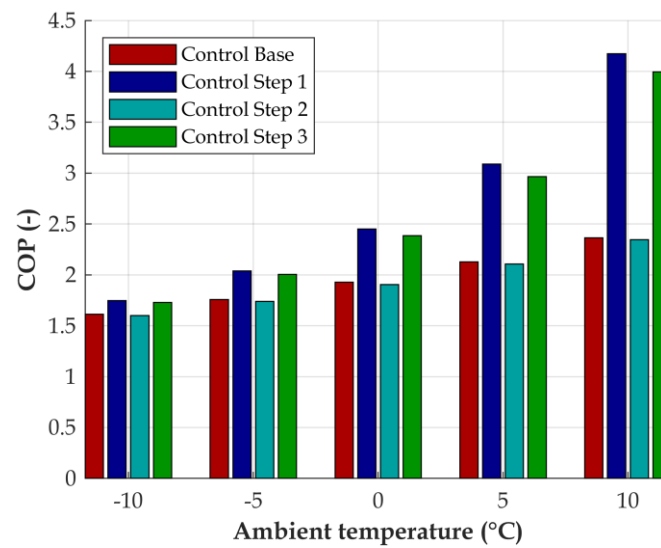


Figure 13. Evaluation of the COP of the optimization steps.

Indeed, Figure 14 presents the results for the COP_{sys} , based on (5). As it can be seen, the total system efficiency of the base scenario (**Control Base**) is largely influenced by the effect of the water pumps and the cabin fan and the COP_{sys} decreases when increasing the ambient temperature. In contrast, the total system efficiency of the optimized scenario (**Control Step 3**) could be significantly increased by up to 81% by applying the demand-based control, especially at mild ambient conditions.

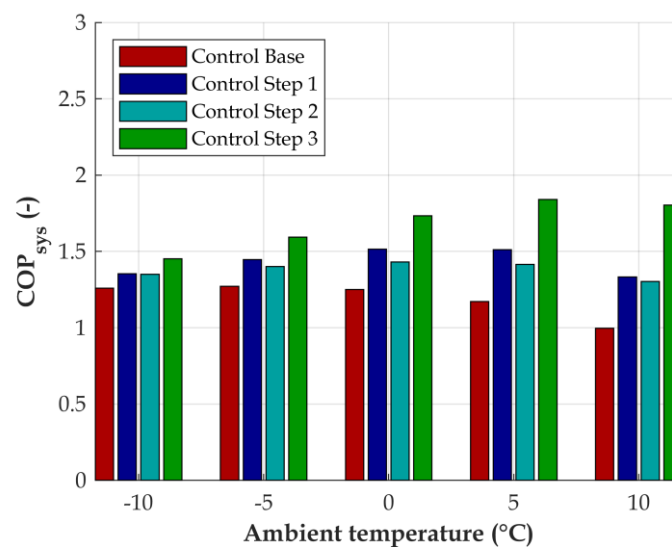


Figure 14. Evaluation of the COP_{sys} of the optimization steps.

Figure 15 compares the climate control system electric load for the various scenarios at different ambient temperatures. It shows a maximum reduction of the electric load of about 287 W in the case of the **Control Step 3** at an ambient temperature of 10 °C.

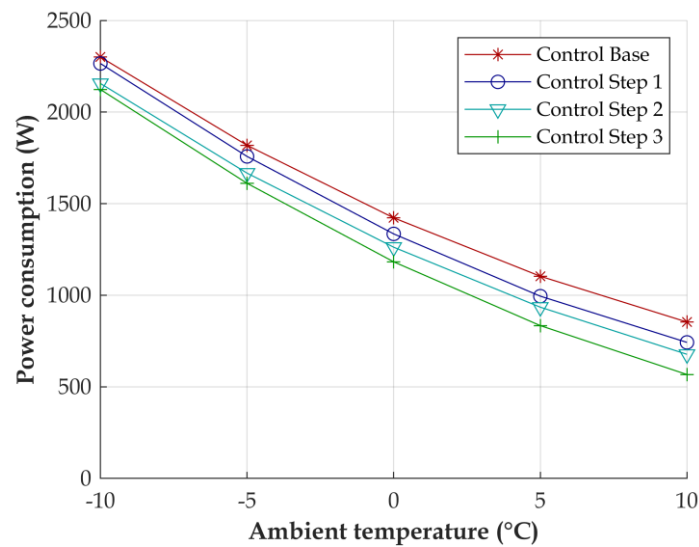


Figure 15. Evaluation of the total power consumption of the optimization steps.

Figure 16 highlights the climate control system savings for the various scenarios at different ambient temperatures. As for both the COP_{sys} and the electric load, savings are more pronounced with higher ambient temperatures. Indeed, the energy savings at an ambient temperature of $-10\text{ }^{\circ}\text{C}$ are respectively for the **Control Steps 1, 2, and 3** of 1.5%, 6.3%, and 7.7% and at an ambient temperature of $10\text{ }^{\circ}\text{C}$ they are of 13.0%, 20.6%, and 33.6%.

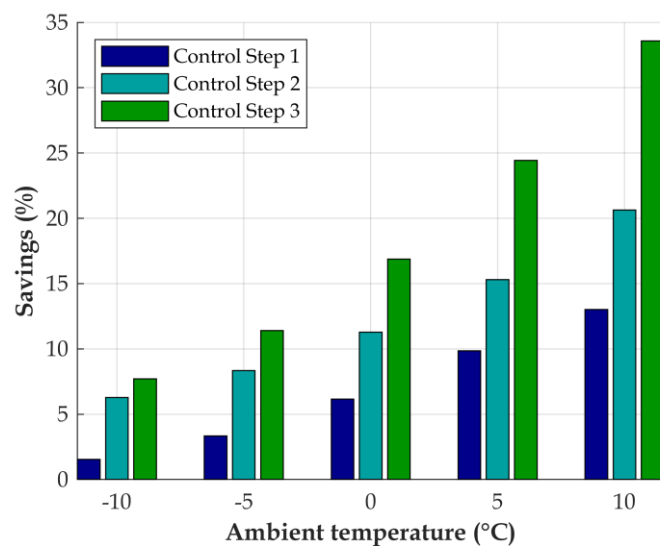


Figure 16. Evaluation of the energy savings of the optimization steps.

Additionally, to validate consistently the developed demand-based control design, the optimal control strategy (**Control Step 3**) has been tested under transient behavior. Indeed, Figure 17 shows the behavior during the first 30 minutes during the heat-up phase starting from various ambient temperatures. For both ambient temperature of $-10\text{ }^{\circ}\text{C}$ and $-5\text{ }^{\circ}\text{C}$ the time to reach the setpoint is unchanged. For temperatures above $0\text{ }^{\circ}\text{C}$ a trade-off between heat-up time and energy efficiency must be found, as at $10\text{ }^{\circ}\text{C}$ the heat-up time increases by 256 s, while at the same time achieving a considerable efficiency increase of 81% and energy savings up to 33.6%.

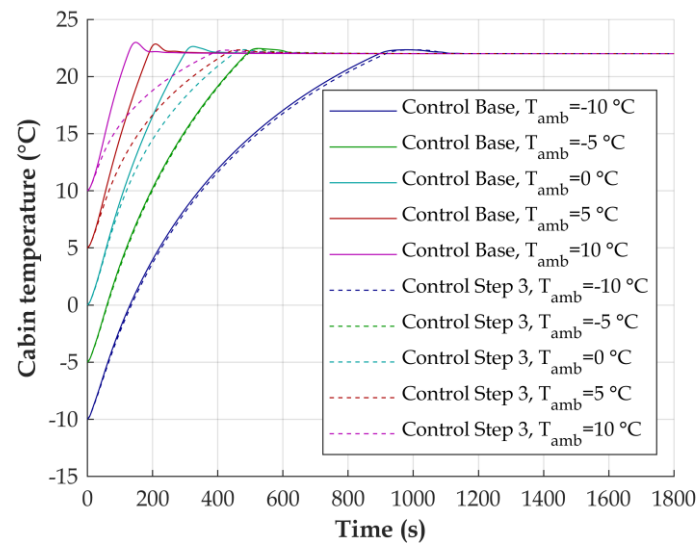


Figure 17. Transient cabin temperature for base- and optimized control.

4. Discussion and Conclusions

This paper shows the applicability of a workflow for using the simulation model of an entire HVAC system to design alternative demand-based operating strategies of the compressor and water pumps toward energy efficient operation. Models have been parameterized based on measurement data on a component level and have used to build up the entire HVAC system model. The validation showed that the HVAC system model can predict accurately the cabin temperature and the HVAC system performance. Finally, the HVAC system model has been used to analyze the efficiency in different operating points (various ambient temperatures) and to derive the optimal controls for operating the compressor and both water pumps with regard to the current heating demand at the maximum efficiency. The study results confirmed that the total energy consumption of the compressor and the pumps can be significantly reduced by up to 34% when adopting the proposed demand-based control strategy.

Summarizing, the proposed demand-based optimal control strategy shows how a relatively simple modification on the software-side (usage of the outdoor temperature value in the existing controllers to define the compressor and water pumps setpoints) can significantly improve the efficiency of the entire system. In that scope, the approach requires a reliable simulation system model, which will play a key role for future research as the energy consumption of the compressor and the pumps can be reduced with minor modifications and shorter development time. That would allow the proposed approach as well to be extended to existing vehicles using a comparable HVAC system set-up. In addition, the workflow could be expanded to include a broader ambient condition range and/or supplementary components to enhance furthermore the HVAC system operating strategy.

Author Contributions: D.D. for the concept; D.D. for the methodology; D.D. for the modelling work; D.D and D.B. for the validation; D.D. for the investigation; D.D. and I.G. for the use case results; D.D. for writing the draft; D.D. and D.B. for reviewing and editing the final draft version. All authors have read and agreed to the published version of the manuscript.

Funding: This project has received funding from the European Union's Horizon 2020 research and innovation programme under grant agreement No. 769826. The content of this publication is the sole responsibility of the Consortium partners listed herein and does not necessarily represent the view of the European Commission or its services.

Conflicts of Interest: The authors declare no conflict of interest.

References

1. New Electric Vehicles. Elektro Auto Mobil, Das Magazine für Elektromobilität, Overview BEV & PHEV, February/March 2019. Available online: <https://www.elektroautomobil.com> (accessed on 16 April 2020).
2. ERTRACT. *European Roadmap Electrification of Road Transport*; ERTRACT: Brussels, Belgium, 2017.
3. Thomas, C.E. *Sustainable Transportation Options for the 21st Century and Beyond*; Appendix A Range Limitations of Battery Electric Vehicles; Springer International Publishing: Cham, Switzerland, 2015; p. 119. [\[CrossRef\]](#)
4. Franke, T.; Rauh, N.; Günther, M.; Trantow, M.; Krems, J.F. Which Factors Can Protect Against Range Stress in Everyday Usage of Battery Electric Vehicles? Toward Enhancing Sustainability of Electric Mobility Systems. *Hum. Factors* **2015**, *58*, 13–26. [\[CrossRef\]](#) [\[PubMed\]](#)
5. Basciotti, D.; Dvorak, D.; Gellai, I. A Novel Methodology for Evaluating the Impact of Energy Efficiency Measures on the Cabin Thermal Comfort of Electric Vehicles. *Energies* **2020**, *13*, 3872. [\[CrossRef\]](#)
6. Shete, K. Influence of Automotive Air Conditioning load on Fuel Economy of IC Engine Vehicles. *Int. J. Sci. Eng. Res.* **2015**, *6*, 1367–1372.
7. Farrington, R.; Rugh, J. Impact of Vehicle Air Conditioning on Fuel Economy, Tailpipe Emissions, and Electric Vehicle Range. In Proceedings of the Earth Technologies Forum, Washington, DC, USA, 31 October 2000.
8. Iora, P.; Tribioli, L. Effect of Ambient Temperature on Electric Vehicles' Energy Consumption and Range: Model Definition and Sensitivity Analysis Based on Nissan Leaf Data. *World Electr. Veh. J.* **2019**, *10*, 2. [\[CrossRef\]](#)
9. Paffumi, E.; Otura, M.; Centurelli, M.; Casellas, R.; Brenner, A.; Jahn, S. Driving Range and Cabin Temperature Performances at Different Ambient Conditions in Support to the Design of a User-Centric Efficient Electric Vehicle: The QUIET Project. In Proceedings of the 14th Conference on Sustainable Development of Energy, Water and Environment Systems 2019, Dubrovnik, Croatia, 1–6 October 2019.
10. Park, J.; Lee, M.; Kim, G.; Park, S.; Kim, J. Integrated Approach Based on Dual Extended Kalman Filter and Multivariate Autoregressive Model for Predicting Battery Capacity Using Health Indicator and SOC/SOH. *Energies* **2020**, *13*, 2138. [\[CrossRef\]](#)
11. Maletić, F.; Hrgetić, M.; Deur, J. Dual Nonlinear Kalman Filter-Based SoC and Remaining Capacity Estimation for an Electric Scooter Li-NMC Battery Pack. *Energies* **2020**, *13*, 540. [\[CrossRef\]](#)
12. Ali, M.U.; Zafar, A.; Nengroo, S.H.; Hussain, S.; Park, G.-S.; Kim, H.-J. Online Remaining Useful Life Prediction for Lithium-Ion Batteries Using Partial Discharge Data Features. *Energies* **2019**, *12*, 4366. [\[CrossRef\]](#)
13. Liang, K.; Zhang, Z.; Liu, P.; Wang, Z.; Jiang, S. Data-Driven Ohmic Resistance Estimation of Battery Packs for Electric Vehicles. *Energies* **2019**, *12*, 4772. [\[CrossRef\]](#)
14. Chen, Y.; He, Y.; Li, Z.; Chen, L. A Combined Multiple Factor Degradation Model and Online Verification for Electric Vehicle Batteries. *Energies* **2019**, *12*, 4376. [\[CrossRef\]](#)
15. Barcellona, S.; Piegari, L. Effect of current on cycle aging of lithium ion batteries. *J. Energy Storage* **2020**, *29*, 101310. [\[CrossRef\]](#)
16. Vatanparvar, K.; Faezi, S.; Burago, I.; Levorato, M.; Al Faruque, M.A. Extended Range Electric Vehicle with Driving Behavior Estimation in Energy Management. *IEEE Trans. Smart Grid* **2018**, *10*, 2959–2968. [\[CrossRef\]](#)
17. Zhang, Z.; Li, W.; Shi, J.; Chen, J. A Study on Electric Vehicle Heat Pump Systems in Cold Climates. *Energies* **2016**, *9*, 881. [\[CrossRef\]](#)
18. Rabl, B. Heat Pump Air Conditioning Systems for Optimized Energy Demand of Electric Vehicles. Comprehensive Energy Management—Safe Adaptation Predictive Control and Thermal Management. In *SpringerBriefs in Applied Sciences and Technology*; Graz University of Technology: Graz, Austria, 2018; pp. 81–92.
19. Ozbek, M.; Gyorog, T.; Hunemorder, W.; Kohli, V.; Caldevilla, A.; Savi, A.; Vitali, D.; Biglia, M.; Nakagawa, M. A compact and efficient water-to-water heat-pump system for electric vehicles. In Proceedings of the 1st International FEV Conference: Zero CO₂ Mobility, Aachen, Germany, 9–10 November 2017.
20. Lajunen, A. Energy Efficiency and Performance of Cabin Thermal Management in Electric Vehicles. *SAE Tech. Pap.* **2017**. [\[CrossRef\]](#)
21. Weustenfeld, T.A.; Bauer-Kugelmann, W.; Menken, J.C.; Strasser, K.; Köhler, J. Heat flow rate based thermal management for electric vehicles using a secondary loop heating and cooling system. In Proceedings of the Vehicle Thermal Management Systems Conference and Exhibition, Nottingham, UK, 10–13 May 2015.

22. Osborne, S.; Kopinsky, J.; Norton, S.; Sutherland, A.; Lancaster, D.; Borgwarner, E.N.; Isenstadt, A.; German, J. *Automotive Thermal Management Technology*; The International Council on Clean Transportation (ICCT): Washington, DC, USA, 2016.
23. Suh, I.-S.; Lee, M.; Kim, J.; Oh, S.T.; Won, J.-P. Design and experimental analysis of an efficient hvac (heating ventilation air-conditioning) system on an electric bus with dynamic on-road wireless charging. *Energy* **2015**, *81*, 262–273. [[CrossRef](#)]
24. Leighton, D. Combined Fluid Loop Thermal Management for Electric Drive Vehicle Range Improvement. *SAE Int. J. Passeng. Cars Mech. Syst.* **2015**, *8*, 711–720. [[CrossRef](#)]
25. Kitanoski, F.; Hofer, A. A contribution to energy optimal thermal management for vehicles. In Proceedings of the IFAC Symposium on Advances in Automotive Control, Munich, Germany, 14 July 2010; pp. 87–92.
26. Fischer, T.; Götz, F.; Berg, L.F.; Kollmeier, H.-P.; Gauterin, F. Model-based development of a Holistic Thermal Management System for an Electric Car with a High Temperature Fuel Cell Range Extender. In Proceedings of the 11th International Modelica Conference, Versailles, France, 21–23 September 2015; pp. 127–133.
27. De Nunzio, G.; Sciaretta, A.; Steiner, A.; Mladek, A. Thermal Management Optimization of a Heat-Pump-Based HVAC System for Cabin Conditioning in Electric Vehicles. In Proceedings of the International Conference on Ecological Vehicles and Renewable Energies, Monte-Carlo, Monaco, 10–12 April 2018.
28. Hosoz, M.; Direk, M. Performance evaluation of an integrated automotive air conditioning and heat pump system. *Energy Convers. Manag.* **2006**, *47*, 545–559. [[CrossRef](#)]
29. Al Faruque, M.A.; Vatanparvar, K. Modeling, analysis, and optimization of Electric Vehicle HVAC systems. In Proceedings of the 21st Asia and South Pacific Design Automation Conference (ASP-DAC), Macau, China, 25–28 January 2016.
30. Hendricks, T.J. *Vehicle Transient Air Conditioning Analysis: Model Development & System Optimization Investigations*; National Renewable Energy Lab. (NREL): Golden, CO, USA, 2001.
31. Lee, H.; Hwang, Y.; Song, I.; Jang, K. Transient thermal model of passenger car’s cabin and implementation to saturation cycle with alternative working fluids. *Energy* **2015**, *90*, 1859–1868. [[CrossRef](#)]
32. Modelica Standard Library. Available online: <https://www.modelica.org/libraries> (accessed on 16 April 2020).
33. TIL Suite. Available online: <https://www.tlk-thermo.com/index.php/en/software/til-suite> (accessed on 16 April 2020).
34. QUIET. Available online: <http://www.quiet-project.eu> (accessed on 16 April 2020).

Publisher’s Note: MDPI stays neutral with regard to jurisdictional claims in published maps and institutional affiliations.



© 2020 by the authors. Licensee MDPI, Basel, Switzerland. This article is an open access article distributed under the terms and conditions of the Creative Commons Attribution (CC BY) license (<http://creativecommons.org/licenses/by/4.0/>).